Weldability of superalloys Hastelloy X by Yb : YAG laser

Jeremie Graneix[1,a], Jean-Denis Beguin[1,b], Joel Alexis[1,c] and Talal Masri[1,d]

[1] Université de Toulouse, LGP, ENIT/INPT, 47 av. d'Azereix, BP1629, 65016 Tarbes cedex, France

[a] Jeremie.graneix@enit.fr, [b] jean-denis.beguin@enit.fr, [c] joel.alexis@enit.fr, [d] talal.masri@enit.fr

Keywords: laser welding, Hastelloy X, microstructure, mechanical properties.

Abstract. Requirements of aircraft parts welded becoming increasingly severe especially in terms of reproducibility of geometry and metallurgical grade of weld bead; laser welding is a viable method of assembly to meet these new demands by its automation to replace longer term the manual TIG welding process. The purpose of this study is to determine the weldability of Hastelloy X alloy by the butt welding process Nd: YAG laser. To identify influential parameters of the welding process (laser power, feed rate, focal diameter and flow of gas) while streamlining testing, an experimental design was established with the CORICO software that uses the graphic correlation method. The position of the focal point was fixed at -1/3 of the thickness of the sheet. The gas flow rate and the power of the beam seem to have a major role on the mechanical properties and geometry of the weld. The strength of the weld is comparable to that of base metal. However, there is a significant drop in the elongation at break of about 30 %. The first observations of the cross section of the weld by scanning electron microscopy coupled with EBSD analysis show generally a molten zone presenting dendritic large grain compared to the equiaxed grains of the base metals without a heat affected zone.

Introduction

Hastelloy X is a commercially available nickel-chromium-molybdenum superalloy with a good oxidation resistance, a good mechanical properties at high temperature and a significant formability; sine qua criteria for the choice of materials for the production of chambers turbojet combustion which is part of this study [1]. Arc welding technique is commonly used for the manufacturing of parts but the aeronautical requirements becoming increasingly severe especially in terms of reproducibility of geometry and metallurgical grade fillet weld. Laser welding is a viable method of assembly to meet these new demands by its automation to replace longer term the manual TIG welding. The high power CO_2 laser is extensively used for practical applications such as cutting and welding laser welding. The CO_2 laser is very used in the industry with regard to Yb:YAG laser which until now was not rather powerful but this changes. The aim of this study was to evaluate the effect of Yb:YAG laser beam parameters on the microstructure and mechanical properties of the laser beam welded superalloys Hastelloy X to define a field of weldability. The implementation of an experimental design approach is required due to the multitude of input parameters and the complexity of the phenomena involved [2-3].

Experimental procedure

Alloy studied is the nickel-chromium-molybdenum alloy Hastelloy X which composition is given in Table 1. The sheet metal is in the annealed condition: it was heat treated between 1150°C and 1175°C and cooled rapidly. Treatment and cooling are carried out under a protective atmosphere [2]. Their thickness is 1.2 mm.

Table 1. Chemical composition of the Hastellloy X (wt %).

Ni	Cr	Co	Mo	W	Al	Fe	Mn	Cu	Si	C
Bal	22.1	1.38	9.0	0.45	0.13	18.7	0.66	0.08	0.35	0.07

The samples *w*ere cut and butt welded by TRUMPH TruLaser Cell 3000 machine. The laser beam is a Yb: YAG TruDisk maximum power 3.3 kilowatts continuous, equipped with a special optical fiber comprising a core fiber 100 µm and a coaxial fiber 400 µm. This fiber thus allows to weld sheet metals with a distributed power density following a classic Gaussian surface (small fiber, SF) either another a torus (large fiber, LF). Two laser parameters are particularly important for welding: the power density of the laser beam and the interaction time. They determine how much energy per area ($W.m^{-2}$) and per unit of time ($J.m^{-2}$) is introduced into the workpiece process [6]. The power density can be controlled by changing the laser power, the size of the focus spot and the configuration of fiber. The interaction time can be adjusted for spot work by changing the irradiation time or by altering the feed rate. To identify influential parameters of the welding process while streamlining testing, an experimental design was established by the CORICO software to understand the new possibilities offered by this new technology [7]. Five parameters were selected for this study: the laser power (500 – 2500 W), the speed welding (1 – 8 $m.min^{-1}$), the focal diameter (110 – 750 µm) which depends on the fiber configuration and the gas flow. The fiber configurations are: the laser beam can be carried by the core of the fiber (SF) or by the periphery of the fiber (LF). The Table 2 presents 30 configurations of welding of the experiment design defined with the software CORICO. The position of the focal point relative to the surface of the sheet has not been considered as a variable parameter. Indeed, much research in this area showed a penetration at a maximum focal length of -1/3 of the thickness of the sheet relative to the surface and this whatever the focal diameter and the feed speed [3].

During the laser welding operation, the specimens were clamped rigidly by a fixture which was designed and manufactured for this study, to align the laser beam with the butt joint and avoid any thermal distortion. To limit the oxidation of the lower face of samples, an argon gaseous protection is realized (20 $l.min^{-1}$).
The microstructures of the base metal and the welds have been studied from observations by optical microscopy (Leica wild M420 stereo microscope) and scanning electron microscopy (FEG-SEM JEOL 7000F). Dimensional limits for specific common imperfections and shape dimensions in laser beam fusion welding are also provided in the referred specifications, in particular, square joints in butt configurations need to be checked in terms of their reinforcement R, low weld LW, drop-thru DT, underfill UF, undercut UC, and shrinkage groove SG. To validate the weldability of these alloys, dimensions of cord section are measured and compared to standard specifications described in EN ISO 6947 (Fig.1).

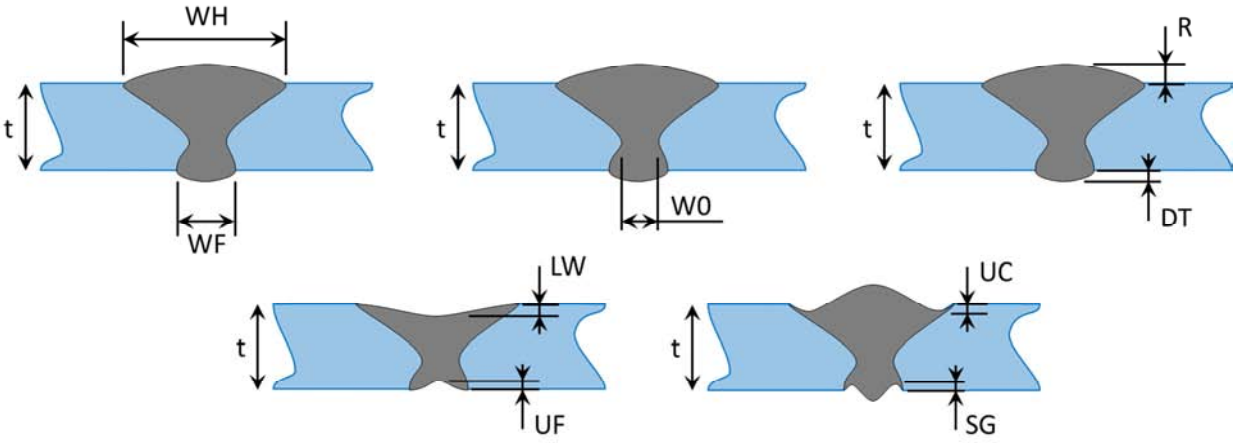

Figure 1. Standart geometrical specifications described in EN ISO 6947.

Table 2. Design matrix defined by the software CORICO.

	Power (w)	Speed ($m.min^{-1}$)	$Ø_{SF}$ (μm)	$Ø_{LF}$ (μm)	Gas flow ($l.mn^{-1}$)
S1	1000	6.25	305	375	25
S2	1500	1.00	110	450	10
S3	2500	8.00	175	525	40
S4	2500	4.50	240	600	32
S5	1500	8.00	240	600	32
S6	1000	6.25	175	525	25
S7	1500	1.00	305	675	32
S8	2000	6.25	175	525	17
S9	2000	8.00	305	675	17
S10	2000	2.75	305	675	40
S11	1000	6.25	240	600	32
S12	2000	4.50	305	675	10
S13	2000	6.25	370	750	40
S14	1500	4.50	370	750	17
S15	1000	2.75	240	600	32
S16	2500	2.75	270	750	17
S17	1500	6.25	110	450	40
S18	500	2.75	175	525	25
S19	2500	1.00	240	600	25
S20	500	4.50	205	675	10
S21	1000	4.50	370	750	17
S22	500	8.00	110	450	25
S23	2000	2.75	175	525	32
S24	1500	4.50	240	600	25
S25	500	8.00	110	450	10
S26	500	1.00	370	750	10
S27	500	1.00	110	450	40
S28	2500	1.00	110	450	10
S29	2500	8.00	370	750	40
S30	500	1.00	110	450	10

A more precise metallurgical study was led for the optimized cords. EBSD analyses were performed using a JEOL 7000F field emission scanning electron microscope at an accelerating voltage of 20 kV equipped with a Nordlys II F+ camera. EBSD analyses were helpful in both analyzing the microstructure of the alloy and the welds. EBSD data were then post-processed with the commercial orientation imaging software package Oxford Channel 5. To minimize measurement errors, all grains comprising less than 3 pixels were automatically removed from the maps before data analysis. A 15◦ criterion was used to differentiate low angle grain boundaries (LAGBs) and high-angle grain boundaries (HAGBs). The grain size was quantified by measurement of grain area (ignoring annealing twin boundaries) and calculation of the equivalent grain diameter assuming each grain as a circle. EDX analysis (oxford Silicon Drift Detector X-Max) were realized to specify the physico-chemical transformations in the welded cords. The mechanical properties of the welds were determined by means of micro-tensile to be compared with those of the parent material.

Results and discussion

The microstructure of the base metal consists of equiaxed grains of average size between 100 and 150 microns for Hastelloy X whatever plane plate studied (Fig.2a). An EBSD analysis was realized in the plan RD-LT of the sheet of Hastelloy X. The figure 1.b present an IPF ZO mapping. Both plats show no texture. Several grains present macles. M_6C's carbides are present in grains and in boundaries grains (Fig. 1c,d)

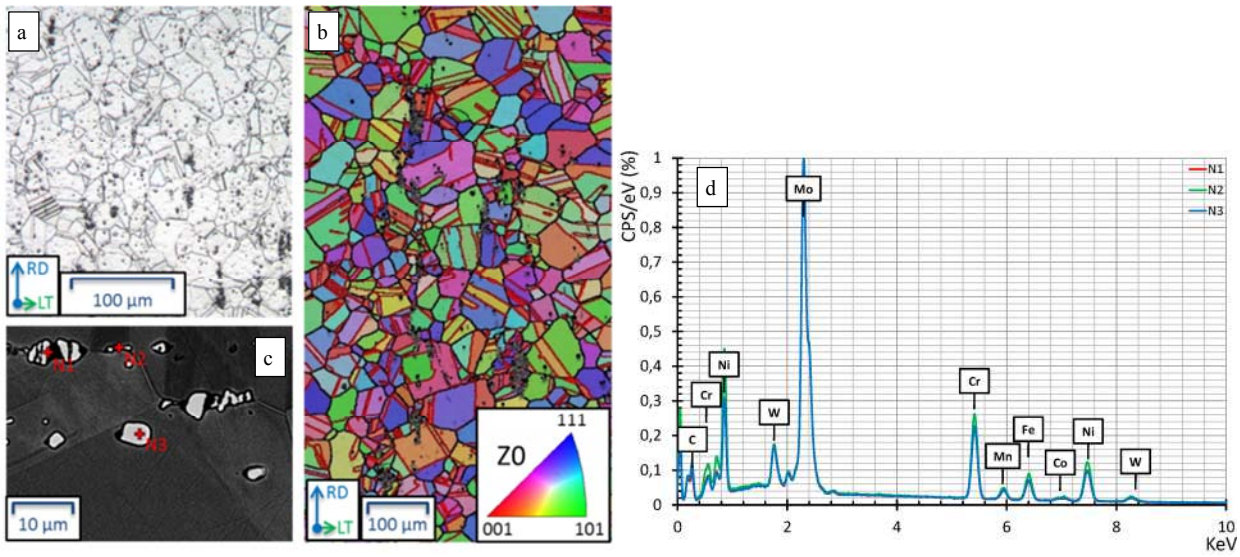

Figure 2. Base metal Hastelloys X (a) Optical microscopy observation. (b) Inverse Pole Figure orientation map (IPF Z0). (c) EDX analyses of M_6C carbide types.

The tensile mechanical properties in different directions in the plane RD-LT have been determined for the base metal (Table 3). No anisotropy of mechanical properties for the two sheets metal is demonstrated confirming previous microstructural observations.

Table 3. Mechanical properties of Hastelloy X.

Angle of orientation with regard to rolling direction	*Rigidity E [GPa]*	*Yield Strength [MPa]*	*Ultimate Tensile Strength [MPa]*	*Elongation [%]*
0°	208±10	446±3	799±2	55±2
45°	211±15	446±11	793±11	53±2
90°	190±20	456±5	806±5	58±8

This study was conducted in several stages with CORICO software: a preliminary study was conducted to determine the limits of weldability defined from geometric criteria fillet weld. A second study clarified the weldability taking into account the mechanical properties of fillet weld and highlights the influence of each parameter on the welding quality of the welded joint. Corico method is based on analysis of partial correlations between all the variables of the experimental design.

The domain of weldability was determined from 30 tries defined by the experimental design for the homogeneous assembly. The figure 3 presents the domains of weldability; that is the domains where the geometrical criteria of cords are verified. The welding speed of 2.75 $m.min^{-1}$ seems the most interesting because the welded cords meet the criteria of the standard about is the diameter of the focal point and for a power superior to 1000 W. For speeds of welding more important, the power must be superior in 1500 W and the focal diameter between 200 and 370 microns. The figure 4a presents the evolution of the mechanical strength of the weld according to the variables: the focal

diameter, the speed of welding and the power. It exists a correspondence enters domain of weldability and the maximal strength of cords. The speed of 2.75 mm.min^{-1} seems to be also the most relevant to obtain the most resistant cords. The break of tensile samples for the same speed is localized in the parent material and not in the welds (Fig. 4b).

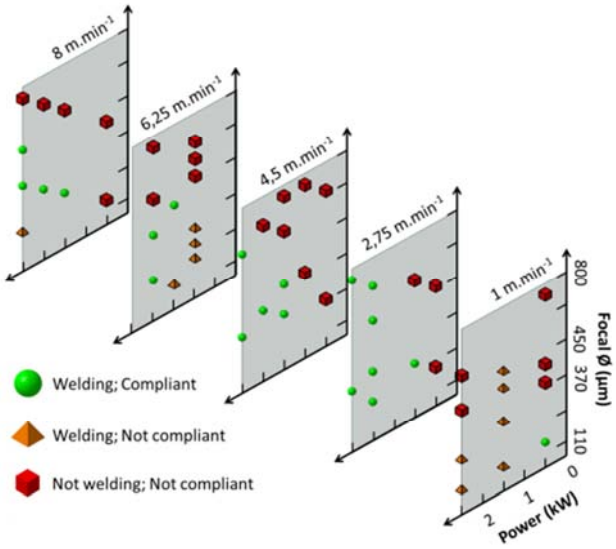

Figure 3. Weldability field of the Hastelloy X.

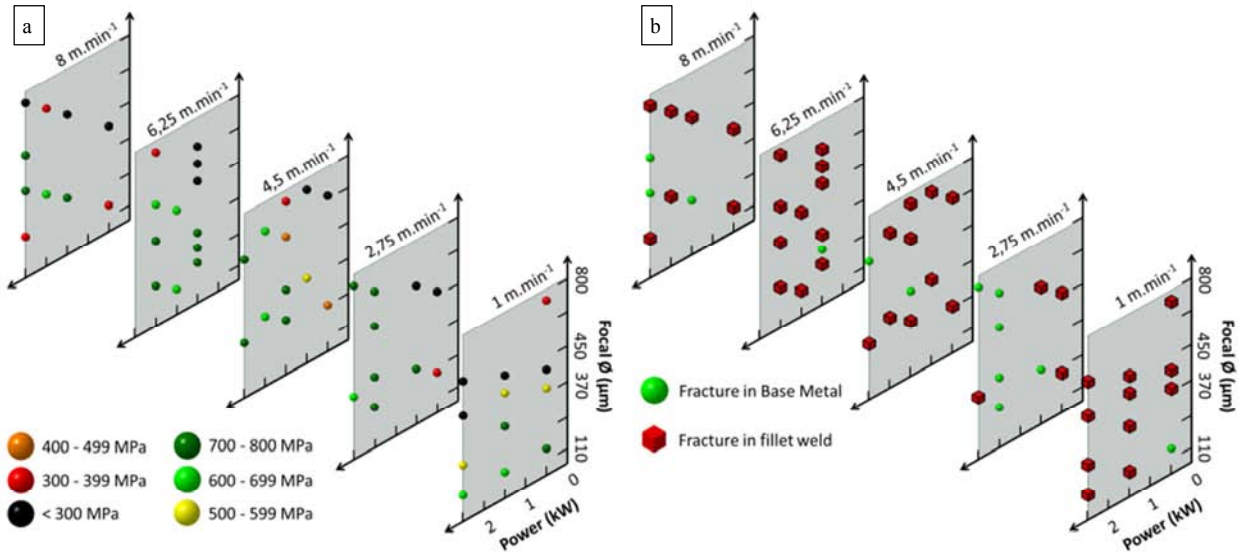

Figure 4. (a) Mechanical propreties field (UTS) of the welds of Hastelloy X. (b) Fracture field of the Hastelloy X welded samples.

The response surface methodology was used to explore the relationships between several explanatory variables (speed, power and focus diameter) and one or more response variables (UTS and elongation).

The figure 4 presents the response surfaces of the ultimate tensile strength according to the experimental variables. The mechanical strength is maximal when the speed of the head is average (of the order of 4.5 m.min^{-1}) and the power superior to 1000 W (Fig. 5a). The focal diameter seems to be a factor of the first order because the strength is maximal for diameters lower than 350 microns whatever the speed and the power (Fig. 5b, c). The response surfaces of the elongation at rupture according to the same variables are presented to the figure 6. The same trends are

highlighted. The maximal elongation is obtained for focal diameters lower than 110 µm, values of power lower than 1500 W and average speeds of welding of the order 4.5 mm.min^{-1}.

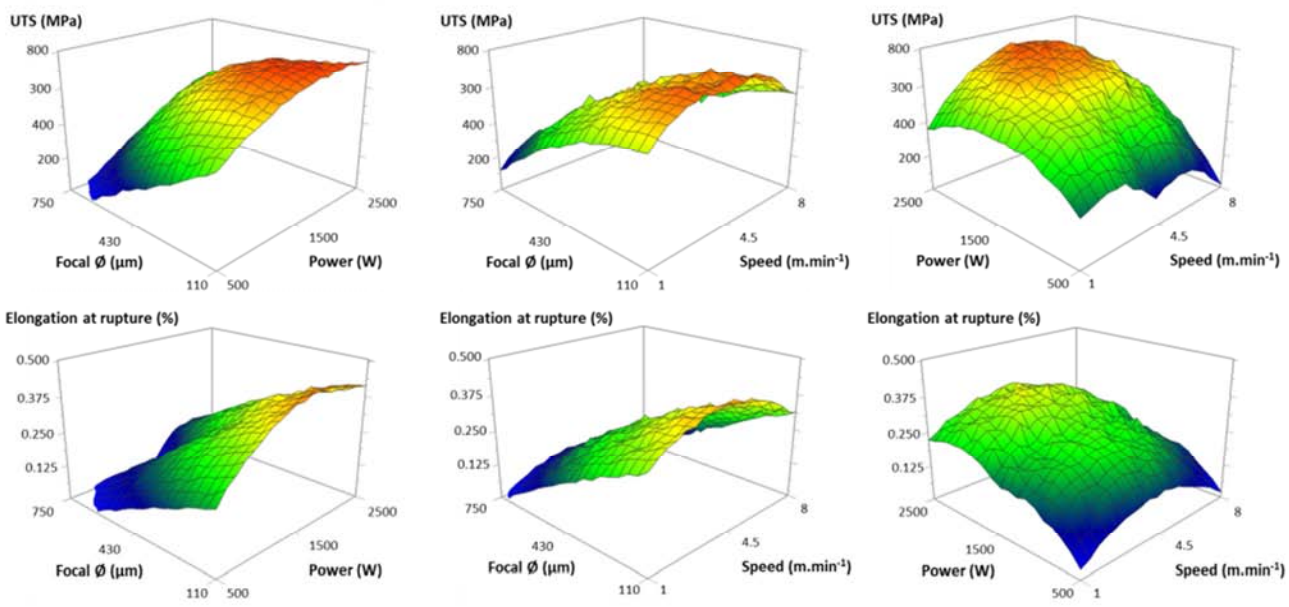

Figure 5. Response Surfaces presenting the evolution of the elongation at rupture according to the welding speed, the power and the focal diameter.

Two optimizations were calculated by the software CORICO by fixing several criteria of desirability. The first optimization was calculated by setting as the standard IN ISO 6947 for the geometrical criteria references and by maximizing the mechanical properties. The second modelling was determined by taking as criteria the maximum of the strength of the welds while trying to minimize the geometrical defects (hollow, gutter) cords. The optimum parameters are summarized in table 4 for the small and large focal diameter for both homogeneous welding.

Table 4. Optimized parameters determined by the software CORICO for homogeneous welding Hastelloy X.

	1st optimization		*2nd optimization*	
	SF	LF	SF	LF
Power (W)	1571	2430	1679	2269
Speed (m.min^{-1})	7.65	3.17	4.67	2.63
Ø focal (µm)	350	518	349	610
Gas flow (l.min^{-1})	40	39	39	39

Microstructure and mechanical properties of these optimized fillet welds were characterized to better understand the influence of welding parameters. Fusion zone shape and final solidification structure of these two alloys were evaluated as a function of laser parameters. The shapes of the weld beads optimized in cross section are shown in Figure 6. A typical form of a Keyhole welding mode is observed for butt weld obtained with small focal, and an X-shaped weld is more representative of a conduction welding method obtained with a large focal. Conduction mode is characterized by a low penetration welds. The weld depth is determined by a combination of heat conduction and convection of the liquid in the solder bath. As against, the mode called keyhole, wherein evaporation and ejection of metal occurs, achieves substantial penetration depths. The dimensions of optimized welds, defined in the figure 1, were measured. All the cords satisfy all the geometrical criteria of the standard IN ISO 6947.

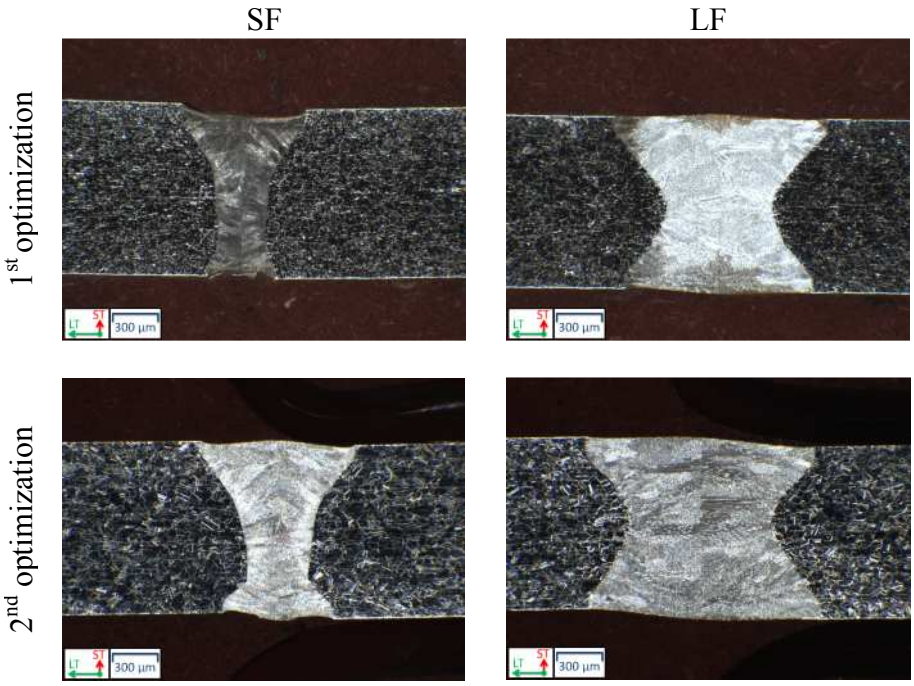

Figure 6. Metallographic observations of welds obtained with the welding optimal parameters.

The strength of the optimized welds was determined from transverse tensile tests. The obtained curves are presented to the figure 7. The curve of the hastelloy X, determined in the same direction, is also given for comparison.

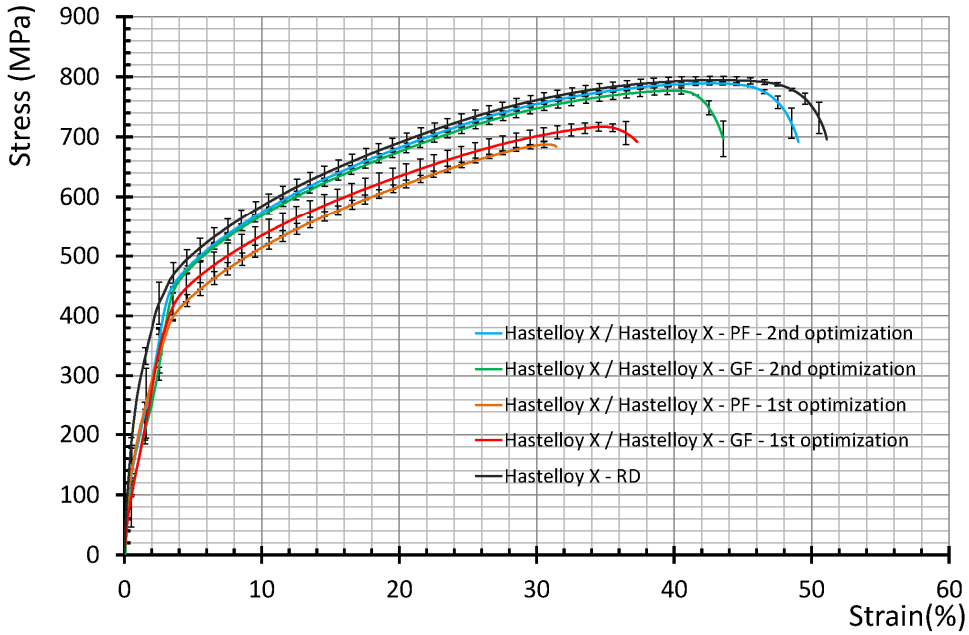

Figure 7. Evolution of the strength of cords according to the strain determined from tensile transverse tests realized on welded test samples.

The mechanical behavior of welded samples with the parameters defined during the first optimization postpones from the mechanical behavior of welded samples with the parameters of the second optimization and the samples of the base material. Whatever focal used to weld the samples of the first optimization, the mechanical strength is lower. This difference of mechanical behavior does not seem due to the size of the weld because the cord which has the best mechanical behavior is the one obtained with the small focal diameter for the conditions of welding defined by

the second optimization. To try to explain the different mechanical behavior of these samples welded, instrumented tensile tests by means of digital correlation images were realised. The local mappings of deformation field of the weld for a global rate of elongation of 21 % of the tensile sample are presented in the figure 8.

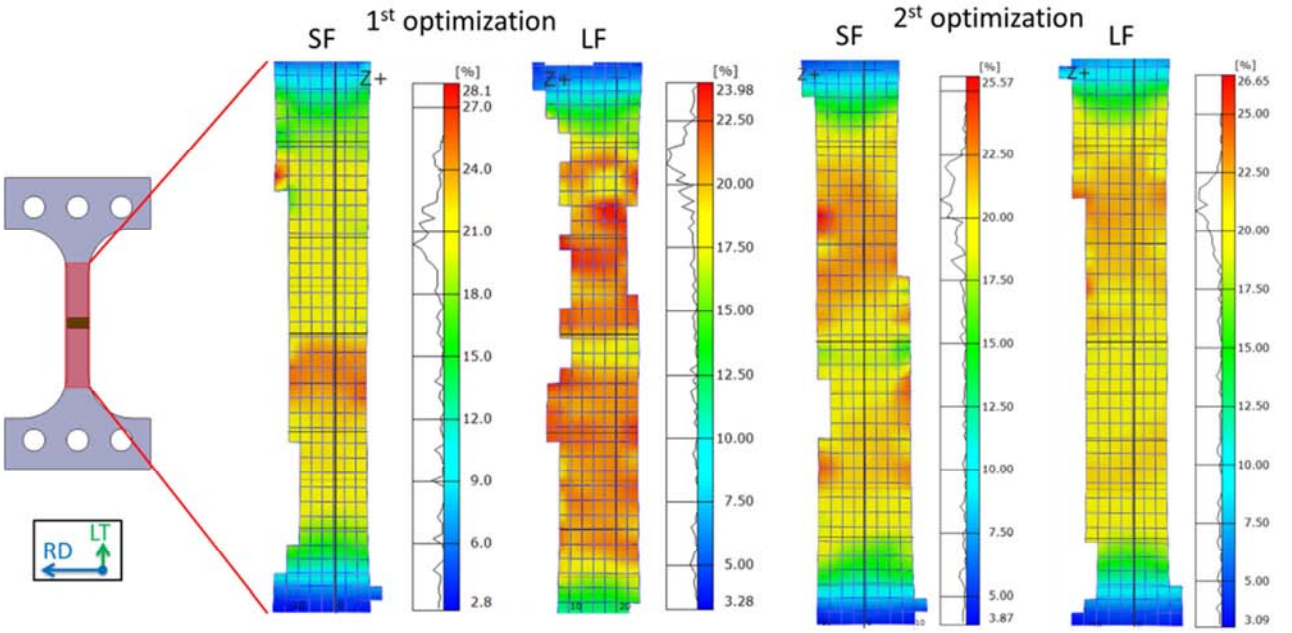

Figure 8. Evolution of the local deformation across the weld for an global elongation of 21% determined by DIC.

Fields of deformation of the sample welded with the small focal of the present first optimization locally a more important rate of deformation due to a concentration of stress in the weld which presents a low weld defect. The sample welded with the large focal of the present first optimization has a less important rate of deformation in the melted zone and uniformly distributed. This can be led by the geometry of the weld which is exempt from defects The premature break is however localized in the melted zone, at the level of the median interdendritic plan. Samples welded with the parameters of the second optimization, whatever is the focal diameter present a rate of homogeneous deformation in the weld and in the parent material. The differences of mechanical behavior of the various welds cannot thus give some explanation only by the geometry of the welded cords; the microstructure in a more local scale thus has to play a very important role.

To verify this hypothesis, EBSD analyses were realized on all the weld in the plan LT-ST. They are presented in the figure 9. These analyses were made in the same conditions as those made for the parent material (FEG-SEM JEOL 7000F coupled with OXFORD Nordlys Fast camera). The observed microstructure presents a growth epitaxic from the parent material of the denditric colonar grains in the melted zone.

Differences of microstructure appear between cords realized with the parameters of the first optimization and the second optimization. Colonnars grains are less disorientated with regard to the axis of tensile tests for the samples of the second optimization. Furthermore, équiaxes grains appear in the center of these melted zones. These differences can explain the best mechanical behavior of these welds.

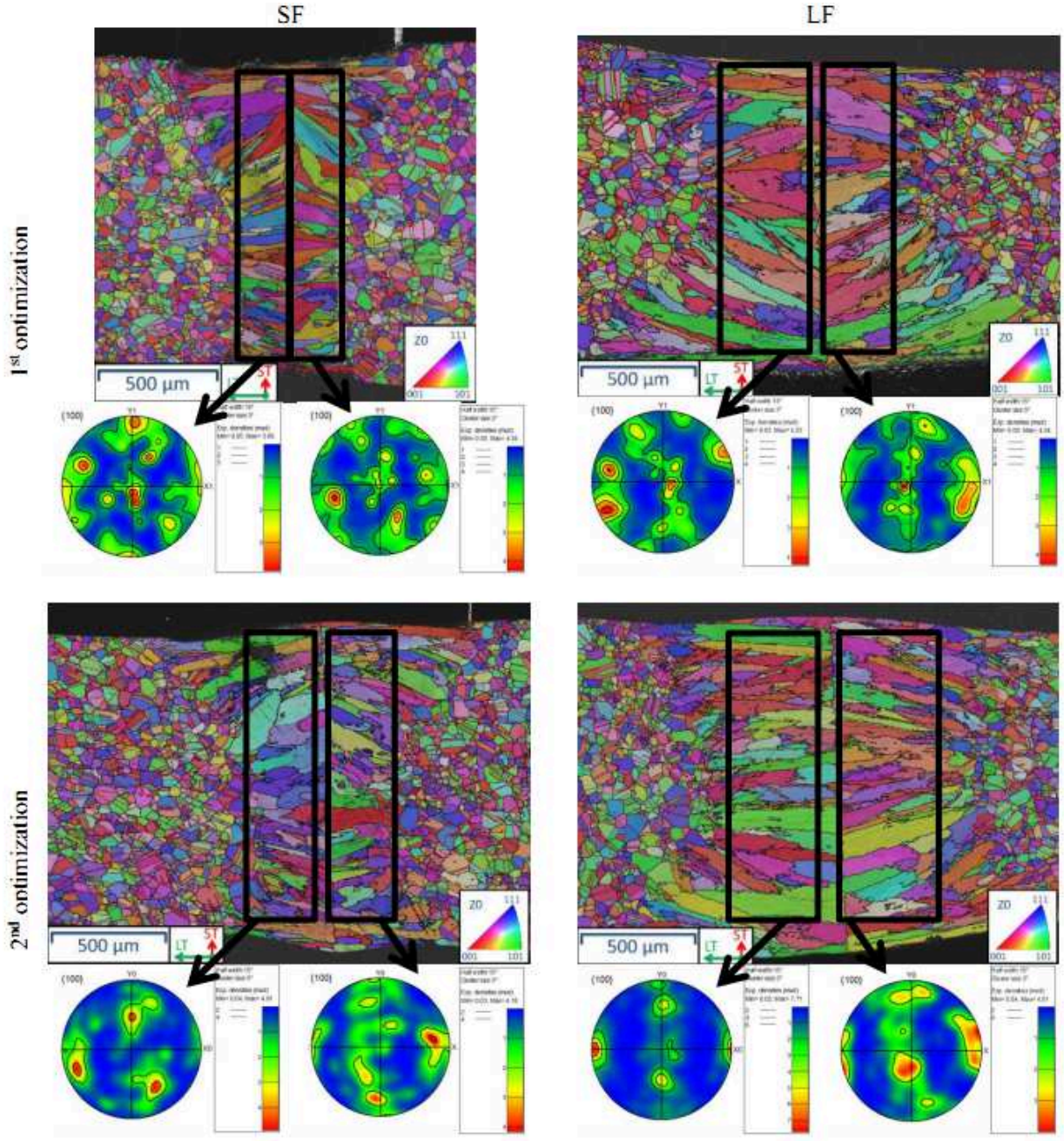

Figure 9. EBSD maps (IPF Z0) of the welds in cross section .

Conclusion

The weldability of Hastelloy X alloy was defined based on welding parameters such as the laser power, the speed, the focal diameter and the gas flow. The most influential parameters seem to be the laser power and the focal diameter. The implementation of experimental design allowed to define two types of optimization. The second optimization based on mechanical criteria seems more interesting than the first optimization based on geometrical criteria of cords. Indeed, the second optimization allows to obtain welds which have similar properties in that of the alloy.

Further analyzes of the carbon and more specifically of the state of precipitation in the weld are planned in order to precise the mechanical behavior of the weld.

References

[1] Hastelloy X alloy, Haynes international report H-3009C, 1997, 1-16.

[2] K.Y. Benyounis, A.G. Olabi, M.S.J. Hashmi, Optic Laser Tech, **40,** 76–87 (2008)

[3] M. Ghoreishi, Int J Adv Manuf Technol, **29**, 70–78 (2006)

[4] M. Moradi, M. Ghoreishi, Int J Adv Manuf Technol, **55**, 205–215 (2011)

[5] B.S. Yilbas, S. Akthar, Int J Adv Manuf Technol, 56, 115–124 (2011)

[6] D. Hitesh Vora, Dilution of molybdenum on aluminum during laser surface alloying, Journal of Alloys and Compounds, **570**, 133-143, (2013)

[7] http://www.coryent.com/corico.html